

Compensation and doping effects in heavily helium-radiated silicon for power device applications

R. Siemieniec^{a,*}, H.-J. Schulze^b, F.-J. Niedernostheide^b, W. Südkamp^c, J. Lutz^d

^a Infineon Technologies Austria AG, Automotive and Industrial, Siemensstraße 2, A-9500 Villach, Austria

^b Infineon Technologies AG, Automotive and Industrial, D-81726 Munich, Germany

^c Infineon Technologies AG, Automotive and Industrial, D-81726 Munich, Germany

^d Aktiv Sensor GmbH, Ruhlsdorfer Str. 95, Gebäude 4, D-14532 Stahnsdorf, Germany

^e Faculty of Electrical Engineering and Information Technology, Technical University of Chemnitz, D-09107 Chemnitz, Germany

Available online 4 November 2005

Abstract

The formation of defects modifying the effective doping concentration of helium-radiated $p^+n^-n^+$ and $p^+p^-n^+$ silicon diodes is analyzed as a function of the annealing temperature. After irradiation with helium at high energy levels and annealing at 220 °C, the probable formation of divacancy clusters increases the number of charged-acceptor states in a space-charge region. Capacitance-Voltage and Spreading-Resistance Profile measurements show that annealing at 350 °C results in the formation of an acceptor-like defect that deep level transient spectroscopy measurements suggest can be tentatively attributed to the V_2O or V_4/V_5 centre. Annealing at 430 °C results in the disappearance of the acceptor-like defect. Instead, pronounced donor formation in a range close to the penetration depth of the helium ions is observed. The influence of these effects on device characteristics is discussed.

© 2005 Elsevier Ltd. All rights reserved.

Keywords: Lifetime control; Recombination centres; Compensation effects; Doping effects; Helium irradiation

1. Introduction

Irradiation techniques are widely used for carrier-lifetime control in bipolar power devices [1–7]. Electron irradiation results in a homogenous distribution of the generated recombination centres, while proton or helium irradiation generates inhomogeneous defect profiles.

It is well-known that proton irradiation followed by annealing in a temperature range between 250 and 500 °C leads to the formation of shallow donors. This effect limits the use of proton irradiation for carrier-lifetime control. The same effect can be used for the creation of deep n -doped regions [8], but sometimes the decreased carrier lifetime in the irradiated area limits such applications.

During helium irradiation, the formation of acceptor-like defects can result in a compensation of the doping concentration. A well-known double acceptor is the divacancy which,

however, is only stable up to annealing temperatures of about 300 °C [9]. In this paper we first focus on doping and compensation effects of helium irradiation after annealing at temperatures ≥ 350 °C. A further increase of the annealing temperature causes the formation of donor-like centres while the recombination centres are vanishing. Finally, the possible formation of divacancy clusters in high-energy helium-radiated silicon annealed at 220 °C is discussed. Consequences for silicon devices are considered.

2. Experimental details

First, $p^+n^-n^+$ (Fig. 1) and $p^+p^-n^+$ (Fig. 2) test diodes were fabricated from FZ (floating zone)-grown silicon. The oxygen concentration in the conventionally prepared diodes was typically higher than 10^{16} cm⁻³. Helium irradiation was performed at room temperature with doses between 7×10^9 and 2.1×10^{12} cm⁻² and energies of 5.4 and 11.6 MeV, respectively. After irradiation, the samples were annealed at $T = 350$ °C or $T = 430$ °C in a nitrogen atmosphere for about 1 h. The doping of the n -type and p -type base material is 6×10^{13} cm⁻² and 3.3×10^{13} cm⁻², respectively.

Fig. 3 shows another test structure that consisted of a p - n junction and a parallel-connected thyristor [7]. The central p -region was surrounded by a p -ring that on one hand acted as

* Corresponding author. Tel.: +43 4242 3056876; fax: +43 4242 3056657.

E-mail addresses: ralf.siemieniec@infineon.com (R. Siemieniec), hans-joachim.schulze@infineon.com (H.-J. Schulze), franz-josef.niedernostheide@infineon.com (F.-J. Niedernostheide), wsuedkamp@aktiv-sensor.de (W. Südkamp), josef.lutz@etit.tu-chemnitz.de (J. Lutz).

Symbols

P	Hole concentration	G	Generation rate
n	Electron concentration	R	Recombination rate
J_n	Electron current density	J_p	Hole current density
N_A^-	Acceptor density	N_D	Donor density
N_A	Ionized acceptor density	N_D^+	Ionized donor density
N_{TA}	Acceptor trap density	N_{TA}^-	Ionized acceptor trap density
N_{TD}	Donor trap density	N_{TD}^+	Ionized donor trap density
V_{TH}	Thermal voltage	E_T	Trap energy level
E_{TA}	Acceptor trap energy level	E_{TD}	Donor trap energy level
f_A	Fraction of occupied acceptor traps	f_D	Fraction of occupied donor traps
n_i	Intrinsic density	E_i	Intrinsic energy level
c_{nA}	Electron capture rate of acceptor traps	c_{pA}	Hole capture rate of acceptor traps
c_{nD}	Electron capture rate of donor traps	c_{pD}	Hole capture rate of donor traps
e_{nA}	Electron emission rate of acceptor traps	e_{pA}	Hole emission rate of acceptor traps
e_{nD}	Electron emission rate of donor traps	e_{pD}	Hole emission rate of donor traps
χ_{nA}	Electron entropy factor of acceptor traps	χ_{pA}	Hole entropy factor of acceptor traps
χ_{nD}	Electron entropy factor of donor traps	χ_{pD}	Hole entropy factor of donor traps
k_B	Boltzmann's constant	q	Elemental charge
t	Time	v_T	Thermal velocity v_T
ϵ_0	Absolute permittivity	ϵ_r	Relative permittivity
L_D	Diffusion length	ϕ	Potential

a field ring, and on other hand was part of the vertical $n^+ - p - n^- - p^+$ structure, forming a thyristor. The p^+ -layer, connecting the $p - n^-$ diode and the concentric p-base of the thyristor, prevented the space-charge region from reaching the surface. Together with the electric field, which is always strongest at the position of maximum curvature of the $p - n^-$ diode (when the p-layer is negatively biased with respect to the n^- -layer), it was ensured that breakdown of the diode occurred in the bulk region. The n^- -substrate was thick enough to ensure that the maximum electric field strength at the $p - n^-$ junction met the avalanche ionization criterion before the field reached the anode p-layer. Thus the avalanche breakdown limited the maximum blocking voltage of the $p - n^-$ diode. The thyristor connected in parallel with the diode protected the diode from

damage due to breakdown. This was achieved by using the avalanche current to trigger the thyristor, which turned on when a certain avalanche current was exceeded. In this case, the voltage drop across the diode was reduced to less than 10 V. The typical avalanche breakdown voltage of the diodes investigated was about 5 kV at room temperature.

The applied irradiation energy of 24 MeV corresponds to a penetration depth of about 300 μm . The irradiated area comprises not only the junction area but also a part of the concentric p-ring (Fig. 3). Local irradiation was performed by irradiating the sample from the upper side through an aluminum mask with a pinhole. The irradiated samples were annealed for 4 h at about 220 $^\circ\text{C}$. Three different helium doses were applied.

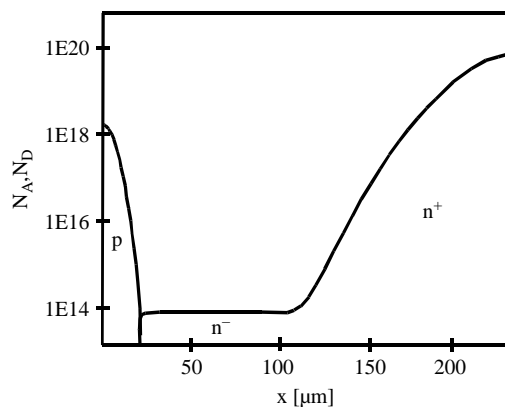


Fig. 1. Doping profile of the $p^+ - n^- - n^+$ diodes ($N_n = 6 \times 10^{13} \text{ cm}^{-3}$)

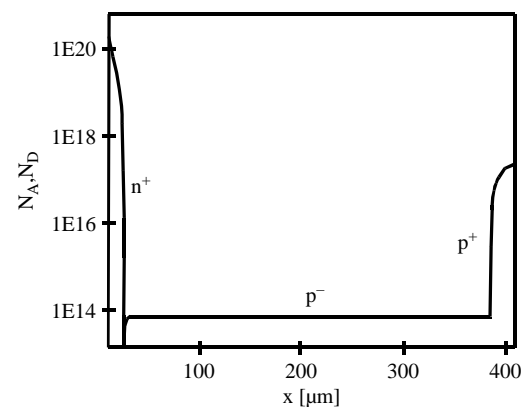


Fig. 2. Doping profile of the $p^+ - p^- - n^+$ diodes ($N_p = 3.3 \times 10^{13} \text{ cm}^{-3}$)

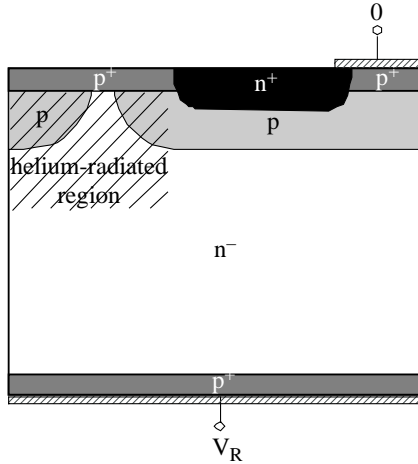


Fig. 3. Radial cross section of a test structure with a p-n⁻ diode (left) in the centre and a ring-shaped thyristor (right) connected in parallel [7].

Table 1 gives an overview of the helium-irradiated samples.

Capacitance-Voltage (CV) measurements, Spreading-Resistance-Profiling (SRP), and Deep Level Transient Spectroscopy (DLTS) measurements were used for defect characterization. The influence of the defects on the device behaviour was studied by analyzing current-voltage characteristics I(V). Forward characteristics were recorded with a high-power Tektronix curve tracer Model 371A by applying a linear voltage ramp for 200 μs. Reverse characteristics were measured with special equipment enabling the application of single sinusoidal half-waves with a period of ≈80 ms and voltage amplitudes up to 10 kV.

3. Device simulation

Irradiation generates centres with different energy levels in the band gap of silicon. Each level may act as an effective recombination centre where the total recombination rate results from the emission and capture processes of each single level. The implementation of this extended model, which includes the complete trap dynamics, is fundamental for an appropriate simulation of such devices [10].

For all simulations, the 2D device simulator TeSCA has been used [11]. This simulation system solves the three fundamental semiconductor equations (the Poisson equation as

Table 1
Sample overview

Sample	Type	Device	Helium irradiation energy (MeV)	Helium irradiation dose (cm ⁻²)
HeND1	n-Si	Diode	11.6	1.4 × 10 ¹²
HeND2	n-Si	Diode	11.6	2.1 × 10 ¹²
HeNS1	n-Si	Diode	5.4	7 × 10 ¹⁰
HeNS2	n-Si	Diode	5.4	7 × 10 ¹¹
HePS	p-Si	Diode	5.4	7 × 10 ⁹
HeNT1	n-Si	Diode & Thyristor	24	3 × 10 ¹¹
HeNT2	n-Si	Diode & Thyristor	24	5 × 10 ¹¹
HeNT3	n-Si	Diode & Thyristor	24	7 × 10 ¹¹

well as the electron and hole current continuity equation). For the consideration of deep levels, additional terms are necessary. In the Poisson Eq. (1), the charged recombination centres are considered. The thermal capture and emission processes of carriers via the deep levels within the band gap lead to additional recombination terms in the continuity Eqs. (2) and (3). The terms R and G refer to further recombination and generation mechanisms such as Auger recombination or avalanche. The occupancies of the acceptor and donor traps are evaluated from the balance Eqs. (4) and (5) according to the relationships of Eqs. (6) and (7). The emission rates are calculated from the position of the recombination centre within the band gap, the capture rates, the entropy factors, and the temperature, as given in Eqs. (8)–(11).

Based on this extended recombination model, the behaviour of radiated devices is predicted with qualitatively and quantitatively good results [4,12].

$$-\text{div}(\varepsilon \cdot \text{grad}\varphi) = q \left[p - n - N_A^- + N_D^+ + \sum (N_{TD}^+ - N_{TA}^-) \right] \quad (1)$$

$$\frac{\partial n}{\partial t} - \frac{1}{q} \text{div} J_n = G - R + \sum \left[e_{nA} N_{TA}^- - c_{nA} n (N_{TA}^- - N_{TA}^-) \right] + \sum \left[e_{nD} (N_{TD}^- - N_{TD}^+) - c_{nD} n N_{TD}^+ \right] \quad (2)$$

$$\frac{\partial p}{\partial t} + \frac{1}{q} \text{div} J_p = G - R + \sum \left[e_{pA} (N_{TA}^- - N_{TA}^-) - c_{pA} p N_{TA}^- \right] + \sum \left[e_{pD} N_{TD}^+ - c_{pD} p (N_{TD}^- - N_{TD}^+) \right] \quad (3)$$

$$\frac{df_A}{dt} = (c_{nA} n + e_{pA})(1 - f_A) - (c_{pA} p + e_{nA})f_A \quad (4)$$

$$\frac{df_D}{dt} = (c_{pD} p + e_{nD})(1 - f_D) - (c_{nD} n + e_{pD})f_D \quad (5)$$

$$N_{TA}^- = N_{TA} \cdot f_A \quad (6)$$

$$N_{TD}^+ = N_{TD} \cdot f_D \quad (7)$$

$$e_{nA} = \chi_{nA} c_{nA} n_i \exp \left[\frac{E_{TA} - E_i}{k_B T} \right] \quad (8)$$

$$e_{pA} = \chi_{pA} c_{pA} p_i \exp \left[\frac{E_i - E_{TA}}{k_B T} \right] \quad (9)$$

$$e_{nD} = \chi_{nD} c_{nD} n_i \exp \left[\frac{E_{TD} - E_i}{k_B T} \right] \quad (10)$$

$$e_{pD} = \chi_{pD} c_{pD} p_i \exp \left[\frac{E_i - E_{TD}}{k_B T} \right] \quad (11)$$

Table 2 gives an overview of the recombination centre parameters determined in previous work [13].

Table 2
Recombination centre properties

Trap	Energy level	Capture rates		Entropy factors	
		c_n (cm ³ /s)	c_p (cm ³ /s)	χ_n	χ_p
$E(90\text{ K})$	$E_C - E_T = 0.169\text{ eV}$	$1.15 \times 10^{-7} \exp\left(-\frac{T}{355.4\text{ K}}\right)$	$6.39 \times 10^{-7} \sqrt{\frac{T}{300\text{ K}}} \exp\left(\frac{6.15 \times 10^{-3}\text{ eV K}}{k_B T}\right)$	0.54	1.85
$E(230\text{ K})$	$E_C - E_T = 0.43\text{ eV}$	$3.41 \cdot 10^{-8} \sqrt{\frac{T}{300\text{ K}}} \exp\left(\frac{22.13 \cdot 10^{-3}\text{ eV}}{k_B T}\right)$	$2.55 \cdot 10^{-5} \cdot T^{-0.84} \frac{1}{\text{K}}$	0.38	2.63
$H(195\text{ K})$	$E_T - E_V = 0.353\text{ eV}$	$9.85 \cdot 10^{-9} \sqrt{\frac{T}{300\text{ K}}} \exp\left(-\frac{85 \cdot 10^{-3}\text{ eV}}{k_B T}\right)$	$4.3 \times 10^{-9} \sqrt{\frac{T}{300\text{ K}}}$	0.25	3.96

4. Compensation effects after annealing at 350 °C

The formation of deep levels in the band gap, caused by helium irradiation, leads to compensation effects that can be observed in CV and SRP measurements. Fig. 4 shows the estimated doping concentration profiles from CV measurements of a diode HNS1 with an n⁻-base for two different annealing temperatures. After annealing at 350 °C a reduction of the estimated doping concentrations is observed at the simulated stopping range of the helium ions.

In contrast to shallow donors and shallow acceptors it is important to point out that CV measurements of samples with deep levels do not allow the direct estimation of free charge carrier densities. CV measurements use a slow reverse voltage sweep and therefore it is only possible to assume a stationary occupation of the deep levels. In the vicinity of the pn-junction, deep acceptor levels are discharged. At the end of the space-charge region (SCR) towards the neutral region, the centres are charged according to the position of the Fermi energy level in the band gap. Once the region with a large local deep acceptor centre concentration is reached, the SCR is extending over the locally compensated region, which results in an estimated doping profile as shown in Fig. 4.

Suitable deep centres, which may cause compensation effects, can be identified using DLTS-measurements.

Minority and majority DLTS spectra of this sample after annealing at a temperature of 350 °C are depicted in Fig. 5. The dominant peaks at $E(90\text{ K})$ and $H(195\text{ K})$ in the two spectra arises from the VO centre and the COVV centre, respectively.

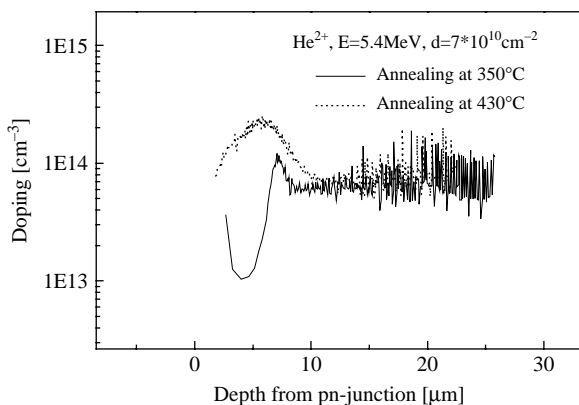


Fig. 4. Doping profile in the n⁻-base of the p⁺-n⁻-n⁺ diode HeNS1 after helium irradiation and annealing for one hour at two different temperatures (CV measurement).

The energy levels of the peaks $E(230\text{ K})$ and $E(130\text{ K})$ are 0.425 and 0.244 eV below the conduction band, respectively. They are close to the energy levels of the singly negative, $V_2^{(0/-)}$, and doubly negative, $V_2^{(-/-)}$ bzw. $V_2^{(-/2-)}$ charge states of the divacancy, which, however, should be already annealed out after annealing at 350 °C. Therefore, we tentatively attribute the two peaks to the singly- and doubly-negative charge states of the V_2O defect, as suggested by the results in [14]. There it has been shown that a double acceptor-like defect with energy levels close to those of the divacancy is formed during divacancy annealing after proton irradiation of low-doped high-resistive oxygenated silicon. Another possible origin of the $E(230\text{ K})$ peak is given in [15], which suggests that the peak arises from a V_4 or V_5 complex.

In sample HeNS1 annealed at 350 °C (Fig. 4), compensation effects are clearly visible at a depth of $\approx 5\text{ }\mu\text{m}$ from the p-n⁻ junction, whereas the background doping in depths $> 10\text{ }\mu\text{m}$ is unchanged. Therefore, the appearance of the centre $E(230\text{ K})$ influences the diode properties not only by modifying the charge-carrier lifetime, but also via compensation effects. Note that the compensation can not be caused by the centre $E(90\text{ K})$, since the Fermi energy level at the background doping of the samples is below the energy level of $E(90\text{ K})$. In p-type silicon, $E(230\text{ K})$ can not be charged since the Fermi energy level is below the energy level of the trap. Therefore, no change in the effective doping occurs (Fig. 6, annealing at $T=350\text{ }^\circ\text{C}$).

DLTS measurements show that most of these centres are annealed out after a temperature treatment at 430 °C for 1 h (Figs. 7 and 8). In particular, the $E(230\text{ K})$ and $E(130\text{ K})$ signals are significantly reduced in the n-type sample HeNS1,

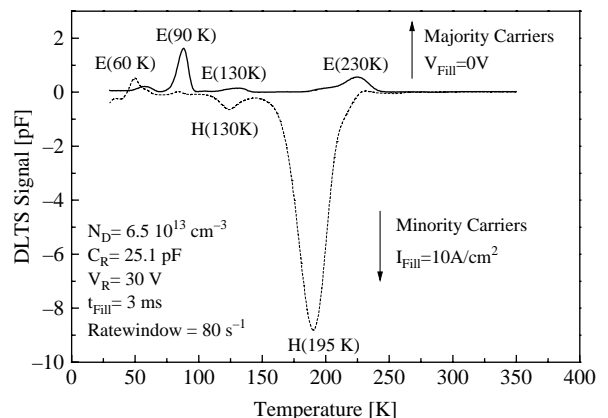


Fig. 5. Minority and majority DLTS spectrum of the p⁺-n⁻-n⁺ diode HeNS1 after helium irradiation and annealing for one hour at $T=350\text{ }^\circ\text{C}$.

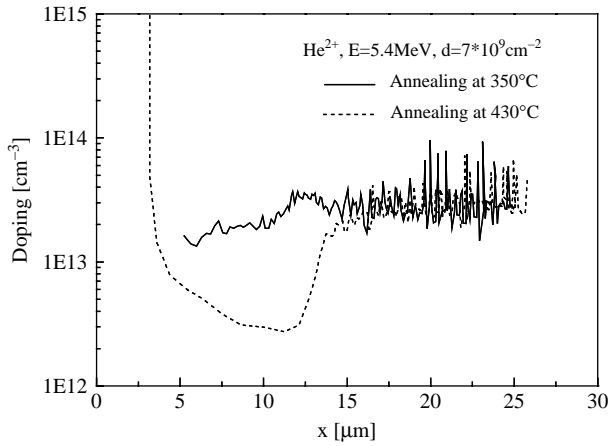


Fig. 6. Doping profile of the $p^+-p^-n^+-n^+$ diode HePS after helium irradiation and annealing for one hour at two different temperatures (CV measurement).

or below the detection limit as in the p-type sample HePS, which has been irradiated with just 10% of the helium dose applied to HeNS1.

Fig. 9 shows the SRP measurements of the samples HeND1 und HeND2. At a depth of $\approx 70 \mu\text{m}$ the doping is decreased, reflecting the reduction of the free-carrier concentration caused by the deep centres. The depth corresponds well to the expected mean penetration depth of the implanted helium ions. Due to the compensation effect, SRP measurements are suitable for the determination of generated defect profiles. A drawback of this technique is that it is difficult to draw conclusions about the defect species or about the exact defect concentrations, as seen by the small difference between the measured effective doping of the two samples depicted in Fig. 9. One inaccuracy arises from the strongly reduced carrier mobility in the ion-stopping region which is not taken into account for the doping calculation from the measured spreading resistance values.

The SRP results confirm that the compensation of the background doping is affected by $E(230 \text{ K})$. The relatively small voltage of several mV that is applied to the sample during the SRP measurements does not cause a strong shift of the

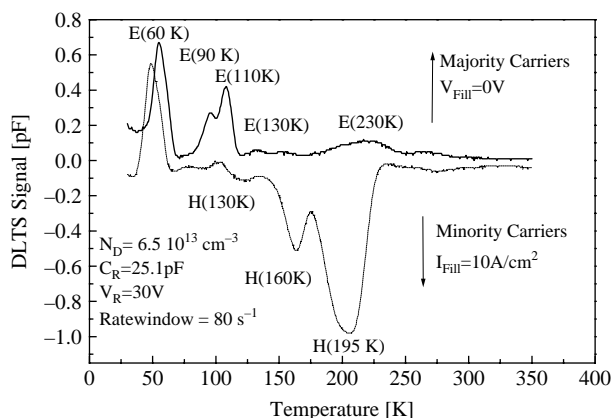


Fig. 7. Minority and majority DLTS spectrum of the $p^+-n^-n^+-n^+$ diode HeNS1 after helium irradiation and annealing for one hour at $T=430 \text{ }^\circ\text{C}$.

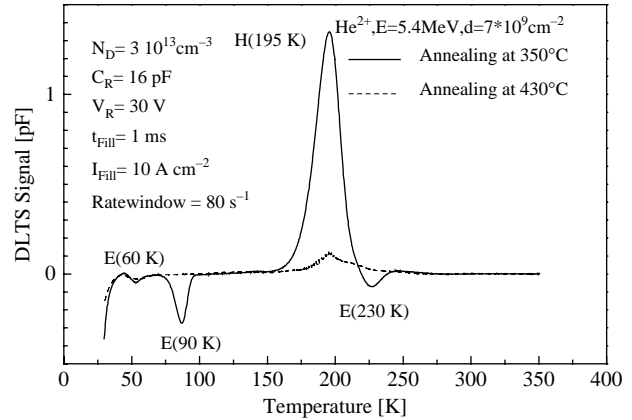


Fig. 8. Minority DLTS spectrum of $p^+-p^-n^+-n^+$ diode HePS after helium irradiation and annealing for one hour at two different temperatures.

Fermi energy level towards the conduction band. Any change in the measured spreading resistance is therefore caused by charged centres $E(230 \text{ K})$.

5. Doping effects after annealing at $430 \text{ }^\circ\text{C}$

CV measurements of the $p^+-n^-n^+-n^+$ diodes after annealing at a temperature of $T=430 \text{ }^\circ\text{C}$ show a higher electron concentration in the helium-irradiated area (Fig. 4), indicating the formation of donors in this area. In the $p^+-p^-n^+-n^+$ diodes, this donor formation results in a reduction of the background p-doping. From Figs. 4 and 6, maximal donor concentrations of $\approx 2.2 \times 10^{14} \text{ cm}^{-3}$ and $\approx 2.7 \times 10^{13} \text{ cm}^{-3}$ in the helium-irradiated area can be estimated for helium doses of 7×10^{10} and $7 \times 10^9 \text{ cm}^{-2}$ after annealing at $430 \text{ }^\circ\text{C}$.

We attribute the formation of these donors in the helium-irradiated area to the formation of Thermal Double Donors (TDDs). TDD formation is well-known from Cz-grown silicon with a high oxygen concentration after annealing, preferably at temperatures between 350 and $500 \text{ }^\circ\text{C}$. They consist of a core, $[110]$ chains of $\langle 001 \rangle$ Si interstitials, surrounded by different shells containing oxygen. Further details concerning TDD formation can be found in Ref. [16].

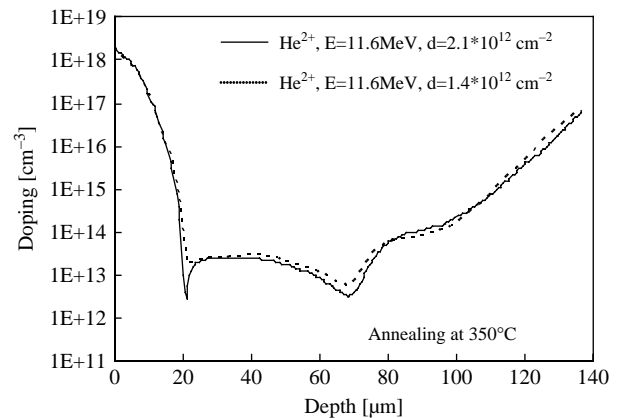


Fig. 9. Doping profile of the helium-radiated $p^+-n^-n^+-n^+$ diodes HeND1 (solid line) and HeND2 (dotted line) after annealing for one hour at $T=350 \text{ }^\circ\text{C}$ (SRP measurement).

In our samples, the oxygen concentration is relatively high due to the preparation conditions of the diodes, which include long thermal diffusion steps (e.g. to create the deep n^+ -layer in the $p^+-n^-n^+$ diodes, cf. Fig. 1). This assumption is also consistent with the existence of $E(60\text{ K})$ in all DLTS spectra (Figs. 5, 7 and 8), since it has been shown that $E(60\text{ K})$ arises from an oxygen-related complex that is found only after long thermal treatment [17].

Similar TDD formation has been observed also in electron-irradiated GTO thyristors fabricated from n-type FZ-grown silicon. The breakdown voltage of these GTO thyristors is limited by the punch-through effect, and reaches a maximum value after annealing at $T \approx 450\text{ }^\circ\text{C}$. From this result it can be concluded that the thermal donor concentration in the n-base of the GTO thyristor has a maximum at this annealing temperature, which is consistent with the well-known TDD formation behaviour in Cz-grown silicon.

It is worth mentioning that DLTS measurements are influenced by the effective background doping concentration due to two effects: First, the maximum detectable defect concentration depends on the background. Second, the spatial resolution of defect profiles determined by making use of the fill-pulse technique [18] is improved for higher doping concentrations. A measure of the spatial resolution [12] is given by the Debye length L_D (Eq. (12)). Thus, under certain conditions, the effect of an increased doping due to helium irradiation can be exploited to improve the spatial resolution of defect profiles

$$L_D = \sqrt{\frac{2\epsilon_r\epsilon_0V_T}{qN_D}} \quad (12)$$

6. Influence on device characteristics

6.1. Influence on forward characteristics

The number of acceptor-states $E(230\text{ K})$ generated in the diodes HeND1 and HeND2 is sufficiently large to cause a clear compensation of the background doping (Fig. 9). This compensation also influences the forward Current–Voltage $I(V)$ characteristics of these devices.

In Fig. 10, the forward characteristics of these samples are shown for different operating temperatures. The measurements were performed using a Tektronix curve tracer Model 371A applying voltage ramps with a length of about $200\text{ }\mu\text{s}$. Due to the generated recombination centres, the forward voltage drop across the device is increased, and the usually unique $I(V)$ characteristic may even change to a characteristic with Negative Differential Resistance (NDR) for low operating temperatures. Such an effect—though only barely detectable—is reflected in the $I(V)$ characteristic at operating temperatures $T=250$ and $T=300\text{ K}$ for the diode HeND2, and $T=250\text{ K}$ for the diode HeND1.

Two mechanisms may account for the appearance of the NDR region. First, similar S-shaped $I(V)$ -characteristics are well-known from Au-doped silicon-pin diodes [19], where

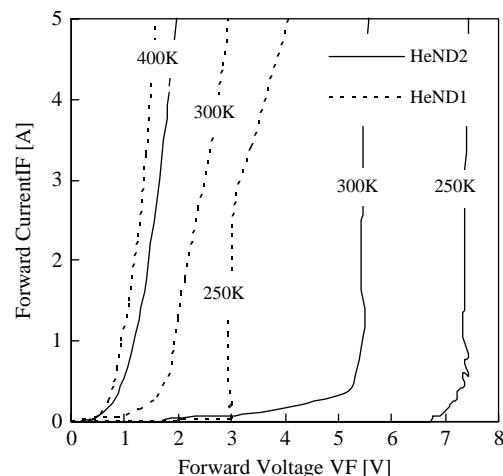


Fig. 10. Measured forward characteristics $I(V_F)$ of samples HeND1 and HeND2.

$c_p > c_n$ of the acceptor-like near midgap level together with the injection-dependent trap occupation causes the bistability. Second, the strong helium irradiation causes so many acceptor-like defects that a certain area of the n^- -base close to the penetration depth of the helium ions is overcompensated and transforms into a p-type region. Therefore, the diode structure changes into a thyristor-like structure for which an S-shaped $I(V)$ characteristic with a NDR-region is well-known. In this case, the observed temperature dependence of the $I(V)$ characteristics in Fig. 10 is due to the dependence on the transistor gain.

It is further shown in Fig. 11 that device simulation is able to predict this behaviour. In these simulations, the voltage was linearly ramped, similar to the measurement. Three centres, $E(90\text{ K})$, $E(230\text{ K})$, and $H(195\text{ K})$, are used for device simulations (cf. table 2). For $E(90\text{ K})$ and $H(195\text{ K})$, parameters matching previous work are used [13]. In $E(230\text{ K})$, the hole capture rate of this trap is modified towards

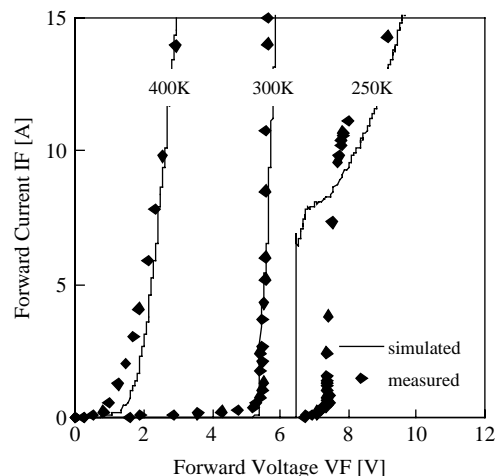


Fig. 11. Comparison of simulated and measured forward characteristics $I(V_F)$ of sample HeND2.

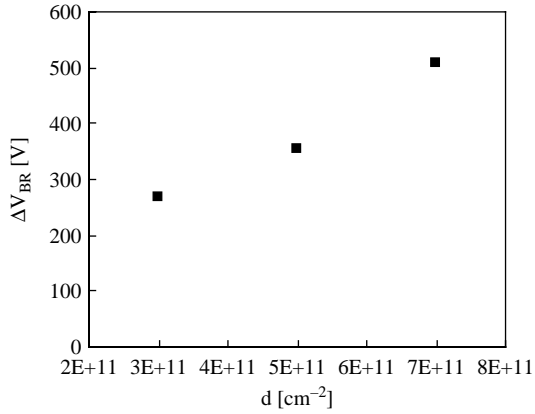


Fig. 12. Increase of forward breakdown voltage of 5 kV p–n⁻ diode test structures HeNT1-3 after 24 MeV helium irradiation at $T=300$ K [7]. Plotted values are mean values from measurements on several samples implanted with the same dose.

a larger effective emission rate as suggested in [20]. The bistable I(V)-characteristic is essentially due to the fact that the ratio of the hole to the electron capture cross section of the $E(230\text{K})$ defect level, c_p/c_n , increases with decreasing operating temperature.

6.2. Influence on blocking voltage

Effects induced by helium irradiation can be exploited for the adjustment of the blocking voltage of p–n⁻ junctions. Fig. 12 shows the increase in the breakdown voltage at room temperature after helium irradiation and annealing at $T=220$ °C as a function of the irradiation dose for the diode test structures HeNT1-3. The breakdown voltage of the diodes increases monotonically with the irradiation dose by several hundred volts. Measurements at 90 °C revealed that the increase in the breakdown voltage is of the same order as at room temperature, so the effect can be applied in power devices operating at elevated temperatures. The low temperature budget during annealing is advantageous, since it enables an adjustment of the breakdown voltage even after the fabrication of a device is completed.

Due to the lower annealing temperature, the acceptor-like divacancy $E(230\text{K})$ still exists and may contribute to compensation effects. In any case, the recombination centres are completely within the SCR region. The number of ionized acceptor-like centres can be estimated with Eq. (13). With a electron-to-hole capture rate ratio c_n/c_p of approximately 0.38, and assuming a rather large peak density of app. $5 \times 10^{14} \text{ cm}^{-3}$ for $E(230\text{K})$, the number of ionized acceptor-like centres is $N_T^- \approx 0.4 \times 10^{-5} N_T \approx 0.4 \times 10^{-10} \text{ cm}^{-3}$. Obviously, the number of ionized centres $E(230\text{K})$ is too small to explain the increase of the blocking voltage.

$$N_T^- = \frac{N_T}{\frac{c_n}{c_p} \exp\left[-\frac{2(E_T - E_f)}{k_B T}\right]} \quad (13)$$

According to [21] the formation of divacancy clusters is possible after irradiation with particles at high doses. Due to

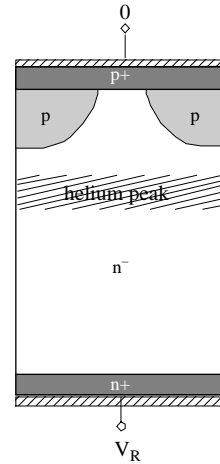


Fig. 13. Simplified structure for device simulation.

the high divacancy concentration ($\approx 10^{20} \text{ cm}^{-3}$) inside the clusters, an interaction of the energy levels between physically different divacancy levels is possible. Due to this interaction, the stationary negatively charged divacancy concentration inside the SCR can increase up to three orders of magnitude. Thus, such cluster formation could explain the significant voltage increase.

A simplified test of this theory by device simulation was performed in the following way: Since the device simulator TeSCA does not provide models which describe the interaction of different deep energy levels, the number of divacancies $E(230\text{K})$ was increased by several orders of magnitude. To keep the carrier lifetimes constant, the capture rates were decreased appropriately, which is possible since the number of charged acceptor-states in Eq. (13) only depends on the ratio of electron-to-hole capture ratio c_n/c_p . Fig. 13 shows the simplified simulation structure, considering only the diode structure. Fig. 14 contains the simulated reverse $I(V_R)$ characteristics, while Fig. 15 depicts the increase of the breakdown voltage with the number of $E(230\text{K})$. The density of charged centres $E(230\text{K})$ along the vertical axis is given in Fig. 16. The simulation result confirms that the expected number of charged divacancies in case of clustering and

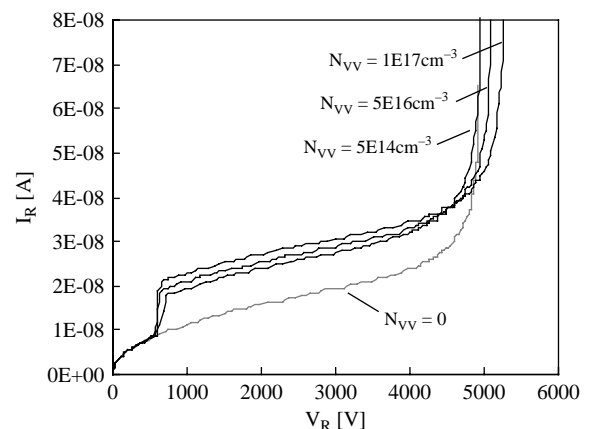


Fig. 14. Simulated reverse characteristics $I(V_R)$ showing the influence of charged divacancies in the SCR.

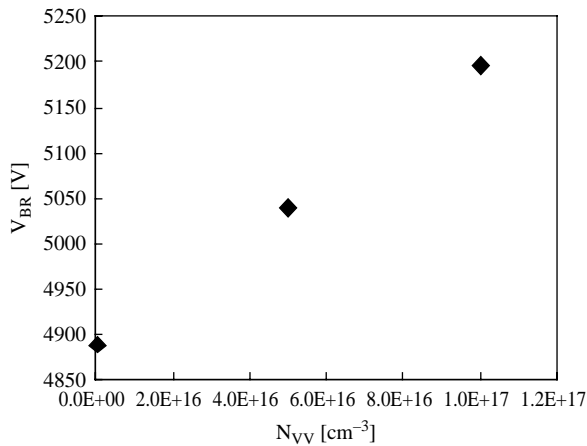


Fig. 15. Increase in the breakdown voltage of the simulation structure in presence of divacancy centres.

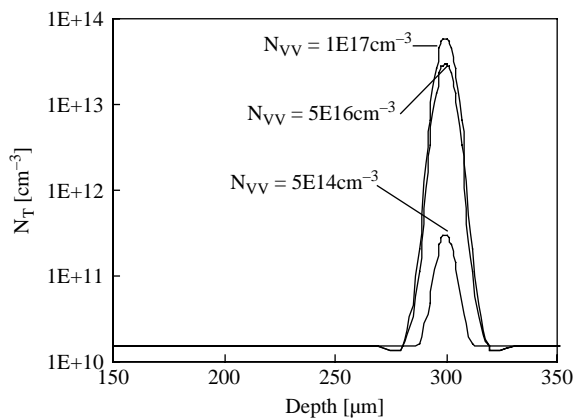


Fig. 16. Density of charged divacancies at breakdown voltage.

interaction of different divacancy levels is adequate for increasing the avalanche breakdown voltage.

7. Conclusion

In this work, the influence of helium irradiation on the background doping has been investigated. Compensation effects were studied by CV, SRP, and DLTS measurements using test diodes based on n-type as well as p-type substrate material. Depending on the annealing conditions, divacancies and the V_2O —respectively V_4/V_5 —defects are assumed to be responsible for the observed compensation effects at annealing temperatures ≤ 350 °C.

At annealing temperatures of 430 °C, we observe an increase in the donor concentration in the area close to the maximum penetration depth of the helium ions. This is most probably caused by the formation of TDDs.

Furthermore it has been shown that helium irradiation can be used to adjust the breakdown voltage of a pn-junction. This effect is most probably related to the formation of divacancy clusters, where interaction of the different divacancy

levels becomes probable due to the large defect densities within. Consequently the total concentration of charged divacancies becomes some orders of magnitude larger than expected by the common assumption of non-clustered divacancy complexes. This assumption is confirmed by device simulations that show that an increase in the number of charged divacancies, while keeping the carrier lifetime constant, results in an increase of the breakdown voltage comparable with that observed experimentally.

Acknowledgements

The authors thank Ms. Becker (SEMIKRON Elektronik GmbH Nürnberg, Germany) for the preparation of the $p^+n^-n^+$ and the $p^+p^-n^+$ diodes and Dr. Möller (Institute Fresenius Dresden, Germany) for performing the SRP measurements and for helpful discussions.

References

- [1] F. Robb, I. Wau, S. Ju, Increasing the switching speed of high-voltage IGBTs Proceedings of the ISPSD, Weimar 1997 pp. 251–254.
- [2] T. Nakagawa, K. Satoh, M. Yamamoto, K. Hirasawa, K. Ohta, 8 kV/3.6 kA light triggered thyristor, Proceedings of the ISPSD, Yokohama 1995 pp. 175–180.
- [3] J. Lutz, Axial recombination centre technology for freewheeling diodes Proceedings of the EPE, Trondheim 1997 pp. 1502–1506.
- [4] R. Siemieniec, J. Lutz, Possibilities and limits of axial lifetime control by radiation induced centres in fast recovery diodes, Microelectronics Journal 35 (3) (2004) 259–267.
- [5] N. Kaminski, N. Galster, S. Linder, C. Ng, R. Francis, 1200 V merged PIN schottky diode with soft recovery and positive temperature coefficient, Proceedings of the EPE, Lausanne 1999.
- [6] J. Vobecký, P. Hazdra, J. Homola, Optimization of power diode characteristics by means of ion irradiation, IEEE Transactions on Electron Devices 43 (1996) 2283–2289.
- [7] F.-J. Niedernostheide, M. Schmitt, H.-J. Schulze, U. Kellner-Werdehausen, A. Frohnmeyer, G. Wachutka, Analysis of radiation-induced defects and performance conditioning in high-power devices, Journal of the Electrochemical Society 150 (1) (2003) G15–G21.
- [8] H.J. Schulze, F.-J. Niedernostheide, M. Schmitt, U. Kellner-Werdehausen, G. Wachutka., Influence of irradiation-induced defects on the electrical performance of power devices, ECS Proceedings 20 (2002) 320–335.
- [9] G.D. Watkins, Vacancies and Interstitials and their interaction with impurities in c-Si Properties of Crystalline Silicon, in: R. Hull (Ed.), EMIS Datareviews Series, London 20 (1999), pp. 643–652. Inspec.
- [10] G.K. Wertheim, Transient recombination of excess carriers in semiconductors, Physical Review 100 (4) (1958) 1086–1091.
- [11] H. Gajewski, B. Heinemann, H. Langmach, TeSCA-Handbuch, Weierstrass-Institute for Applied Analysis and Stochastics, Berlin, 1991.
- [12] R. Siemieniec, Simulation von Leistungsbau-elementen mit durch Bestrahlungsverfahren eingestellter Trägerlebensdauer, Ph.D. thesis TU Ilmenau, BoD Verlag Norderstedt, 2003.
- [13] R. Siemieniec, F.-J. Niedernostheide, H.-J. Schulze, W. Südkamp, U. Kellner-Werdehausen, J. Lutz, Irradiation-induced deep levels in silicon, EMIS Proceedings, Hawaii, 5, 2004 pp. 369–384.
- [14] E.V. Monakhov, B.S. Avset, A. Hallen, B.G. Svensson, Formation of a double acceptor centre during divacancy annealing in low-doped high-purity oxygenated Si, Physics Review B 65 (2002) 233207.
- [15] J. Guldberg, Electron trap annealing in neutron transmutation doped silicon, Applied Physics Letters 31 (9) (1977) 578.

- [16] C.A.J. Ammerlaan, Thermal double donors in c-Si in: R. Hull (Ed.), *Properties of Crystalline Silicon EMIS Datareviews Series vol. 20* (1999) Inspec, pp. 663–668.
- [17] S.D. Brotherton, P. Bradley, Defect production and lifetime control in electron and gamma-irradiated silicon, *Journal of Applied Physics* 53 (8) (1982) 5720–5732.
- [18] W. Südkamp, W. Gerlach, *Untersuchung tiefer Zentren und Bauelementesimulation, VDI/VDE-IT - Reihe Innovationen in der Mikrosystemtechnik* 1999.
- [19] I. Dudeck, R. Kassing, The influence of recombination data on the I-V characteristics of silicon p-i-n diodes, *Journal of Applied Physics* 48 (11) (1977) 4786–4790.
- [20] P. Hazdra, J. Rubeš, J. Vobecký, Divacancy profiles in MeV helium irradiated silicon from reverse I-V measurement, *Nuclear Instruments and Methods in Physics Research B* 159 (1999) 207–217.
- [21] K. Gill, G. Hall, B. MacEvoy, Bulk damage effects in irradiated silicon detectors due to clustered divacancies, *Journal of Applied Physics* 82 (1997) 126–136.